Electronic Supporting Information (ESI)

Improved Solubility of Titanium-Doped Polyoxovanadate Charge Carriers for Symmetric Non-aqueous Redox Flow Batteries

Mamta Dagar,[a] *D. M. M. Mevan Dissanyake,*[a] *Daniel N. Kesler,*[a] *Molly Corr,*[a] *Joshua D. McPherson,*[a] *William W. Brennessel,*[a] *James R. McKone,*[b] *and Ellen M. Matson*[*a]

[a]Department of Chemistry, University of Rochester, Rochester, NY 14627, USA

[b]Department of Chemical and Petroleum Engineering, University of Pittsburgh, Pittsburgh, PA 15261, USA

Email: matson@chem.rochester.edu

Supporting Information Table of Contents

Experimental methods:

Determining D_0. 5 mM concentration of the cluster ($[Ti_2V_4O_5(OMe)_{14}]$, **Ti_2V_4TRIOL^B**, and **Ti_2V_4TRIOL^C**) with 0.1 M $[^nBu_4N][PF_6]$ as the supporting electrolyte were used for all experiments. CV measurements were carried out inside a nitrogen filled glove box (MBraun, USA) using a Bio-Logic SP 150 potentiostat/galvanostat and the EC-Lab software suite. Cyclic voltammograms were recorded using a 3 mm diameter glassy carbon working electrode (CH Instruments, USA), a Pt wire auxiliary electrode (CH Instruments, USA), and a Ag/Ag^+ non-aqueous reference electrode with 0.01 M $AgNO_3$ in 0.1 M $[^nBu_4N][PF_6]$in CH_3CN (Bio-Logic). Cyclic voltammograms were *iR* compensated at 95% with impedance taken at 100 kHz using the ZIR tool included within the EC-Lab software.

The diffusion coefficient associated with each redox couple was determined by using the slope of the peak current (i_p) versus the square root of scan rate $v^{1/2}$. The Randles – Sevcik equation was used to estimate the diffusion coefficients from CV data. For a reversible redox couple, the peak current is given by the Eqn S1:

$$i_p = 2.69 \times 10^5 \, n^{3/2} \, A \, c \, D_0^{1/2} \, v^{1/2} \qquad \text{Eqn S1}$$

In eq. S1, n is the number of electrons transferred; A is the electrode area (0.0707 cm^2 for the glassy carbon working electrode); c is the bulk concentration of the active species; D_0 is the diffusion coefficient of the active species; ν is the scan rate. For an irreversible redox couple, the peak current, is given by the Eqn S2:

$$i_p = 2.99 \times 10^5 \, n^{3/2} \, \alpha^{1/2} A \, c \, D_0^{1/2} \, v^{1/2} \qquad \text{Eqn S2}$$

where α is the charge transfer coefficient. For this study, α = 0.5.

For the redox couples that show quasi-reversible kinetics, relationships for both reversible and irreversible redox reaction are usually employed to determine the diffusion coefficients of such redox processes. Therefore, an average value of diffusion coefficient was approximated for a quasi-reversible redox couple using both equations S1 and S2.[1-3]

Calculation of k_0. The electron-transfer kinetics was estimated directly from CV measurements by using the Nicholson method.[4] The potential difference (ΔEp) of oxidation and reduction peaks were obtained at different scan rates. The transfer parameter, ψ, was extracted from the working curve constructed by Nicholson using ΔEp values. The standard heterogeneous charge-transfer rate constant, k_0, for a given electron transfer process was determined using Eqn S3:

$$\Psi = \nu^{-1/2} k_0 \left(\pi n F D_0 / RT\right)^{-1/2} \qquad \text{Eqn S3}$$

where n is the number of electrons transferred, F is the Faraday constant, D is the diffusion coefficient, ν is the scan rate, R is the ideal gas constant and T is the temperature.

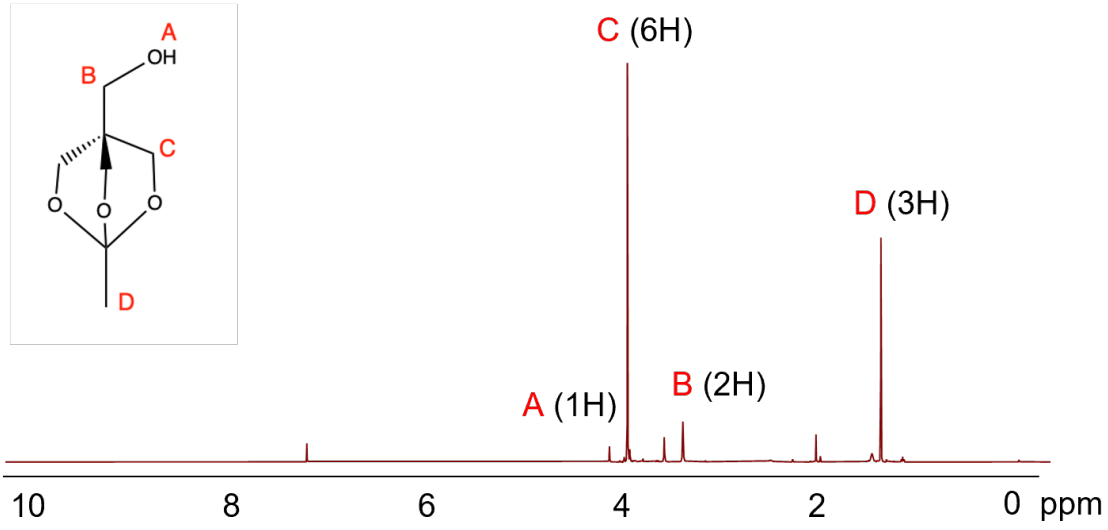

Figure S1. ^{1}H NMR spectrum of the Protected Ligand Precursor (PLP).

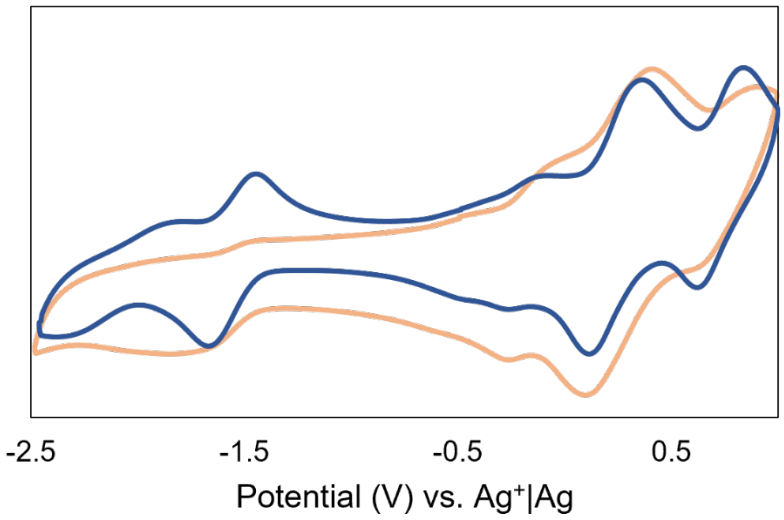

Figure S2. CVs of the crude reaction mixture of **Ti_2V_4TRIOL^{B}**. The blue trace denotes the product obtained for the solution phase, whereas the orange trace depicts the solid precipitate retrieved from the reaction mixture.

Table S1. Crystallographic parameters for molecular structure of **Ti_2V_4TRIOL^B**.

Empirical formula	C_{17} H_{44} O_{20} Ti_2 V_4
Formula weight	868.08
Temperature	99.98(10) K
Wavelength	1.54184 Å
Crystal system	orthorhombic
Space group	*Pna*2$_1$
Unit cell dimensions	*a* = 18.8039(2) Å α = 90° *b* = 16.2998(2) Å β = 90° *c* = 10.42640(10) Å γ = 90°
Volume	3195.69(6) Å^3
Z	4
Reflections collected	122147
Independent reflections	6812 [*R*(int) = 0.0943]
Observed reflections	6387
Completeness to theta = 74.504°	100.0%
Absorption correction	Multi-scan
Max. and min. transmission	1.00000 and 0.05775
Refinement method	Full-matrix least-squares on F^2
Data / restraints / parameters	6812 / 1 / 401
Goodness-of-fit on F^2	1.073
Final *R* indices [*I*>2sigma(*I*)]	*R*1 = 0.0510, *wR*2 = 0.1377
R indices (all data)	*R*1 = 0.0547, *wR*2 = 0.1433
Absolute structure parameter	0.360(11)
Largest diff. peak and hole	1.246 and -0.706 e.Å^{-3}

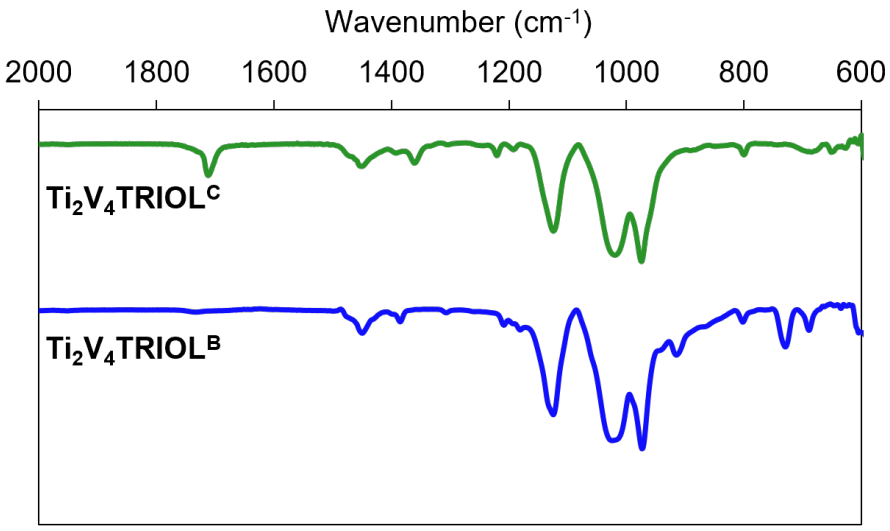

Figure S3. IR spectra of **Ti_2V_4TRIOL^B** (**blue**, bottom) and **Ti_2V_4TRIOL^C** (**green**, top).

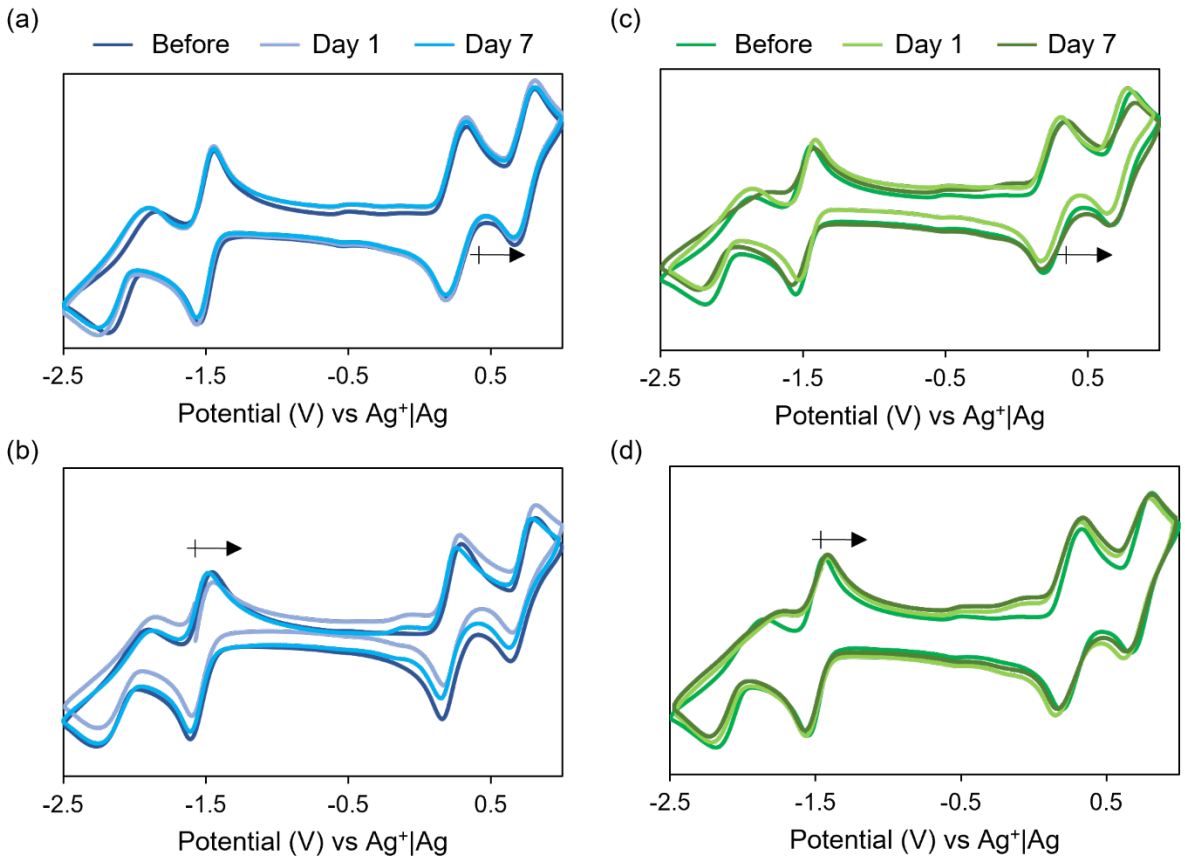

Figure S4. CV monitoring of the (a) bulk oxidized and (b) reduced solutions of **Ti_2V_4TRIOL^B**. Voltammograms in (c) and (d) represent the corresponding data for **Ti_2V_4TRIOL^C**. Arrows indicate the open circuit voltage post bulk electrolysis.

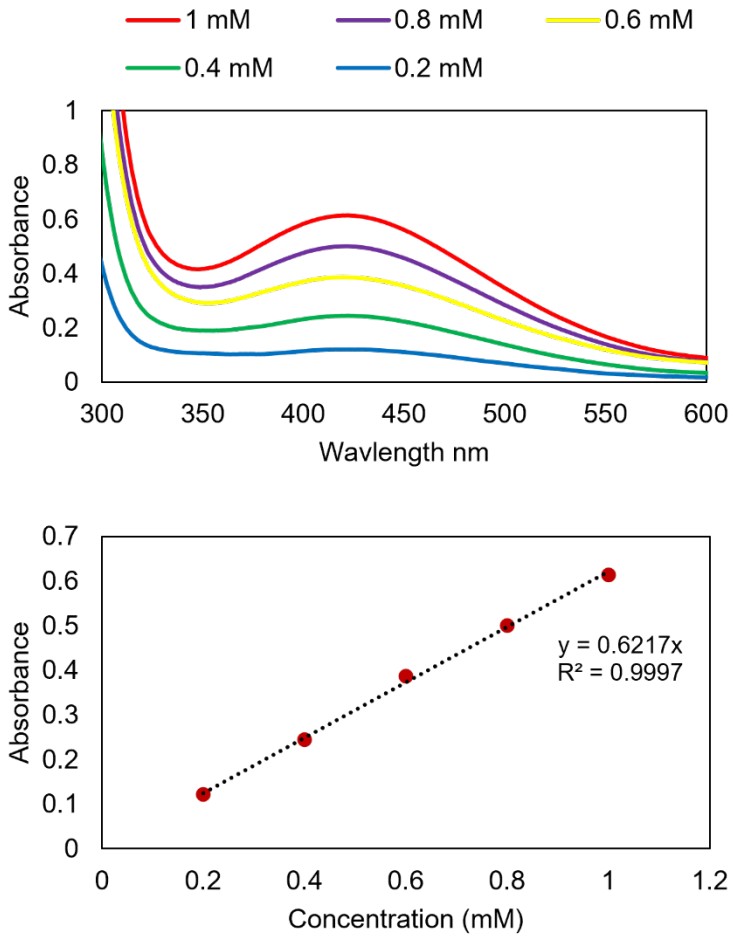

Figure S5. Calibration curve for solubility of $\mathbf{Ti_2V_4TRIOL^B}$ in acetonitrile with 0.1 M [^{n}Bu$_4$N][PF$_6$].

Table S2. Solubility measured for $\mathbf{Ti_2V_4TRIOL^B}$ in acetonitrile with 0.1 M [^{n}Bu$_4$N][PF$_6$]. Peak absorbance values at 422 nm were used to generate a calibration curve, with molar absorptivity, ε = 656 M^{-1} cm^{-1}.

Trials	Absorbance at 422 nm	Diluted concentration (mM)	Saturated concentration (mM)
1	0.4758	3.06	306.12
2	0.4621	2.97	297.31
3	0.5525	3.53	353.86

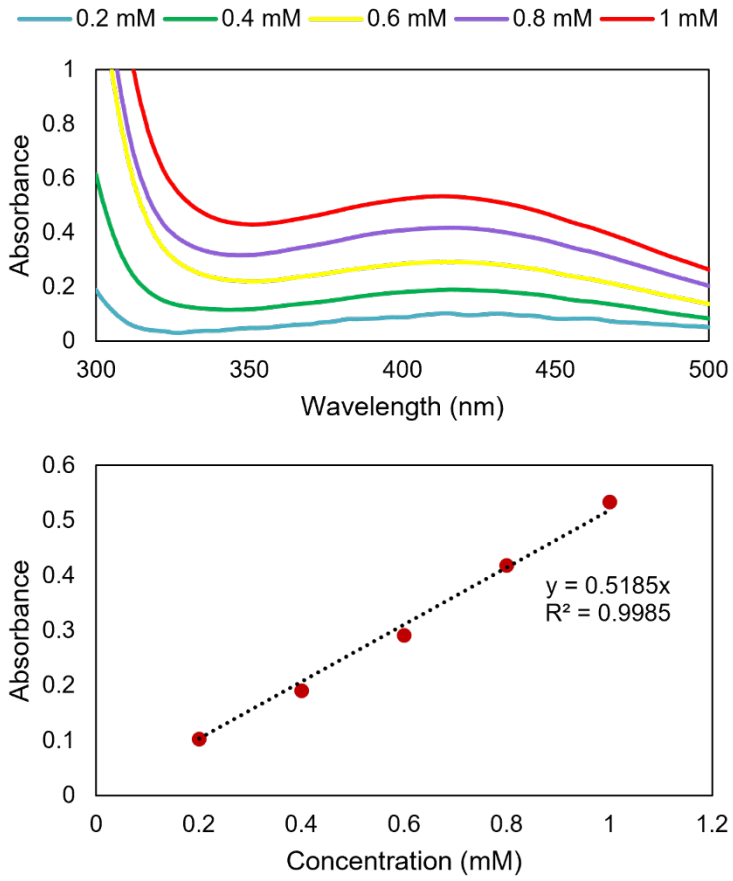

Figure S6. Calibration curve for solubility of **Ti_2V_4TRIOL^C** in acetonitrile with 0.1 M [^{n}Bu$_4$N][PF$_6$].

Table S3. Solubility measured for **Ti_2V_4TRIOL^C** in acetonitrile with 0.1 M [^{n}Bu$_4$N][PF$_6$]. Peak absorbance values at 415 nm were used to generate a calibration curve, with molar absorptivity, ε = 877 M^{-1} cm^{-1}.

Trials	Absorbance at 415 nm	Diluted concentration (mM)	Saturated concentration (mM)
1	0.8385	6.46	646.86
2	0.8347	6.43	643.92
3	0.8791	6.78	678.18

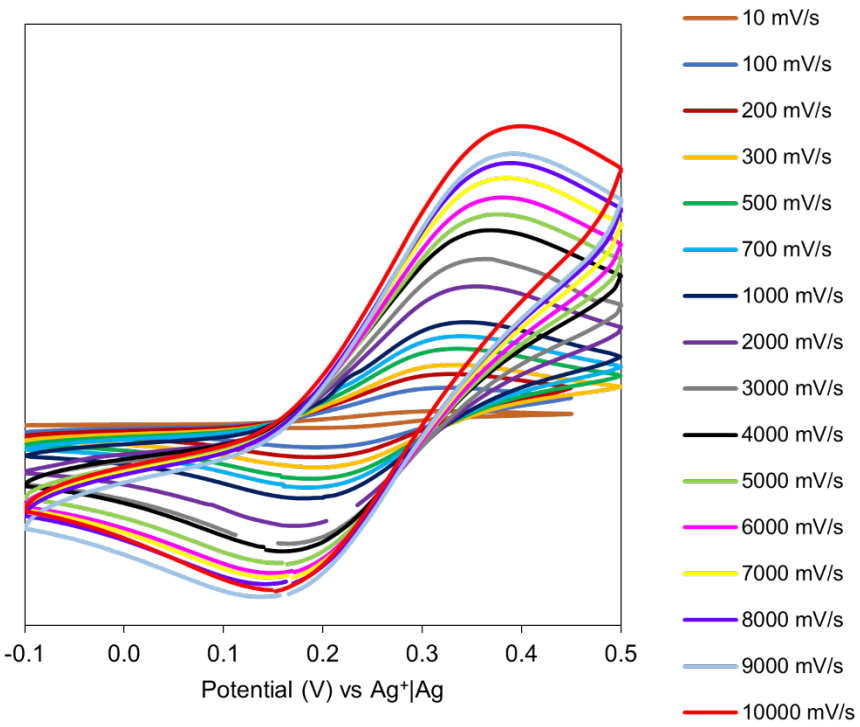

Figure S7. Cyclic voltammograms of $\mathbf{1^{+}/0}$ redox couple of $\mathbf{Ti_2V_4TRIOL^B}$ at scan rates ranging from 10 – 10000 mV/s in acetonitrile.

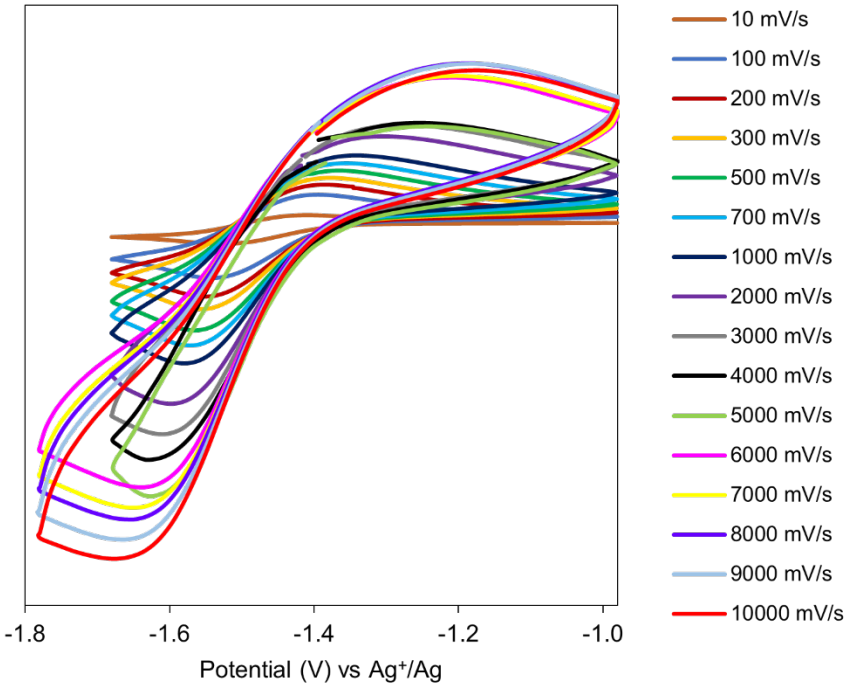

Figure S8. Cyclic voltammograms of $\mathbf{0/1^{-}}$ redox couple of $\mathbf{Ti_2V_4TRIOL^B}$ at scan rates ranging from 10 – 10000 mV/s in acetonitrile.

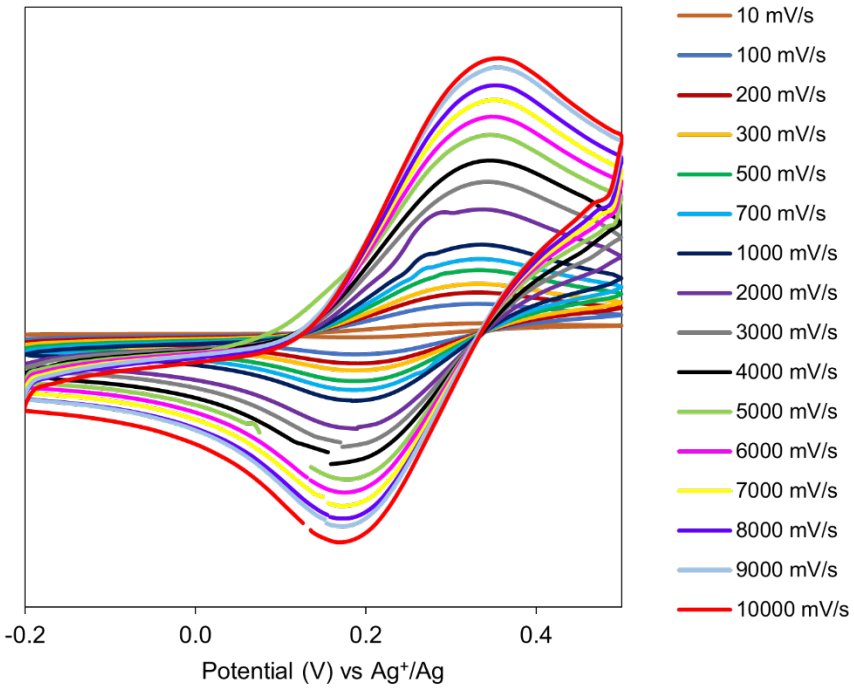

Figure S9. Cyclic voltammograms of **1^{+}/0** redox couple of **Ti$_2$V$_4$TRIOL^{C}** at scan rates ranging from 10 – 10000 mV/s in acetonitrile.

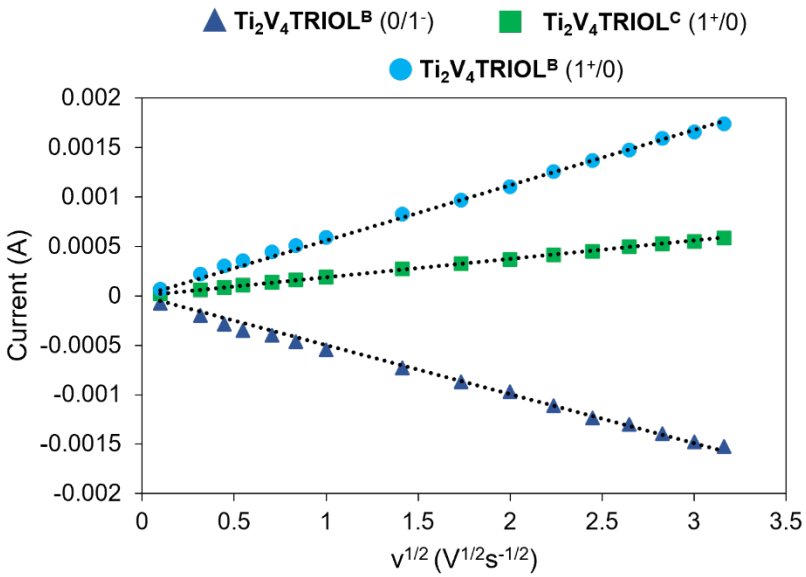

Figure S10. Plot of current vs (scan rate)$^{1/2}$ for **Ti$_2$V$_4$TRIOL^{B}** and **Ti$_2$V$_4$TRIOL^{C}** for each redox couple. **1^{+}/0** denotes one electron oxidation; **0/1^{-}** denotes one electron reduction.

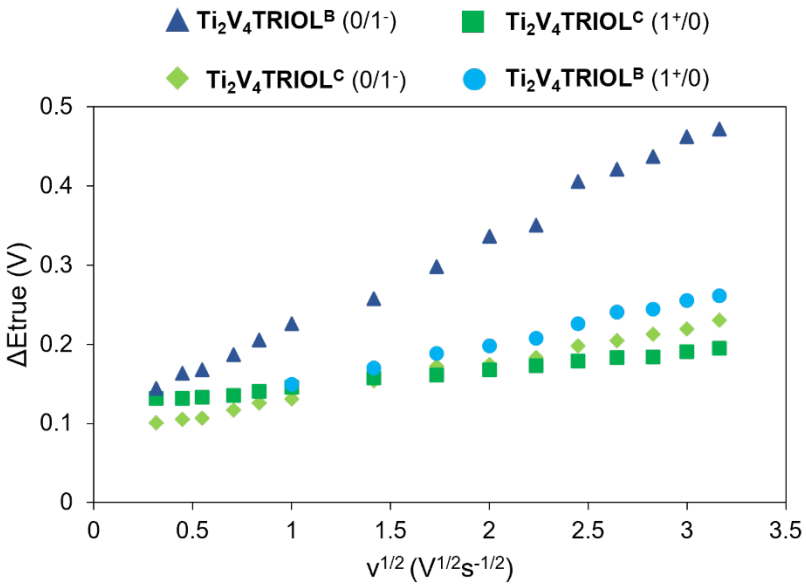

Figure S11. Plot of ΔE_p vs (scan rate)$^{1/2}$ for **Ti_2V_4TRIOL^B** and **Ti_2V_4TRIOL^C**.

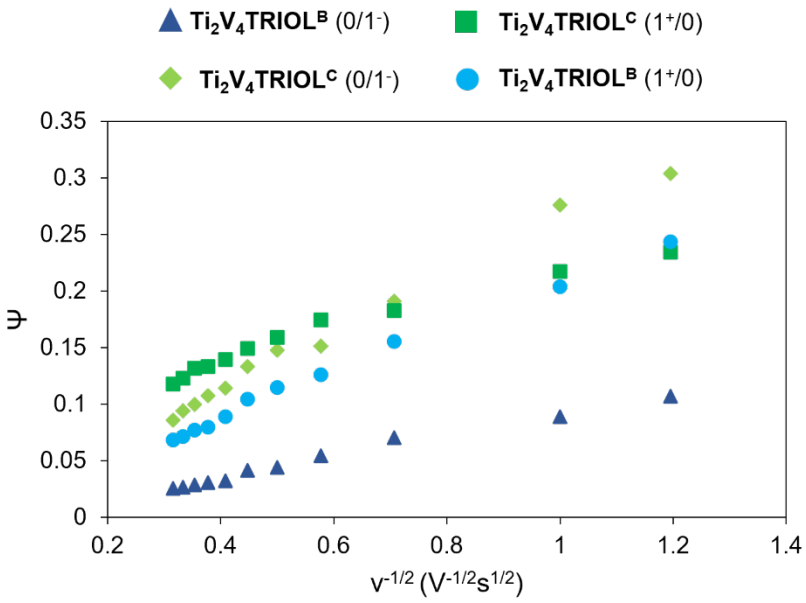

Figure S12. Plot of Ψ vs (scan rate)$^{-1/2}$ for **Ti_2V_4TRIOL^B** and **Ti_2V_4TRIOL^C**.

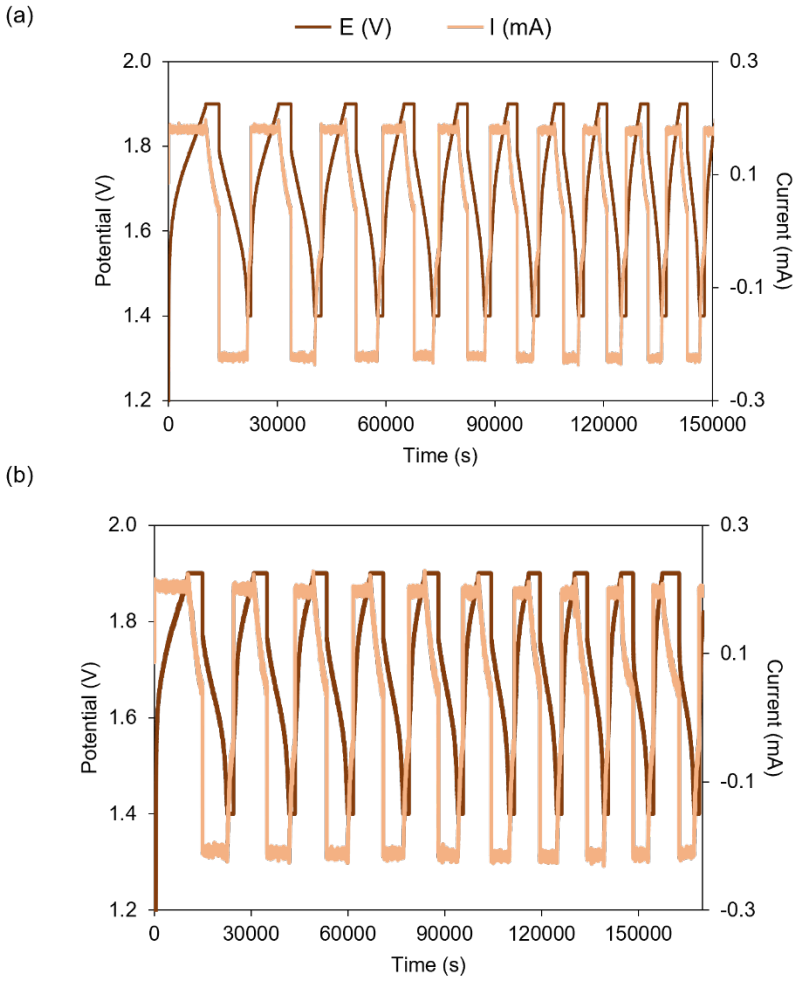

Figure S13. Full voltage trace of the charge-discharge behavior of (a) **Ti_2V_4TRIOL^B** (b) **Ti_2V_4TRIOL^C** for 10 cycles.

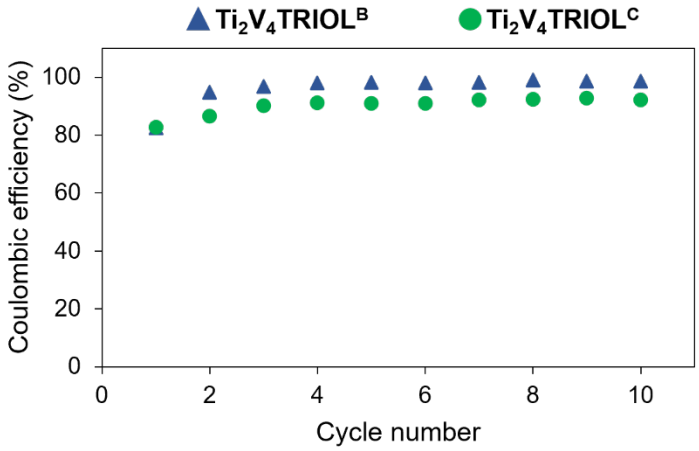

Figure S14. Coulombic efficiencies of **Ti_2V_4TRIOL^B** and **Ti_2V_4TRIOL^C** during battery cycling.

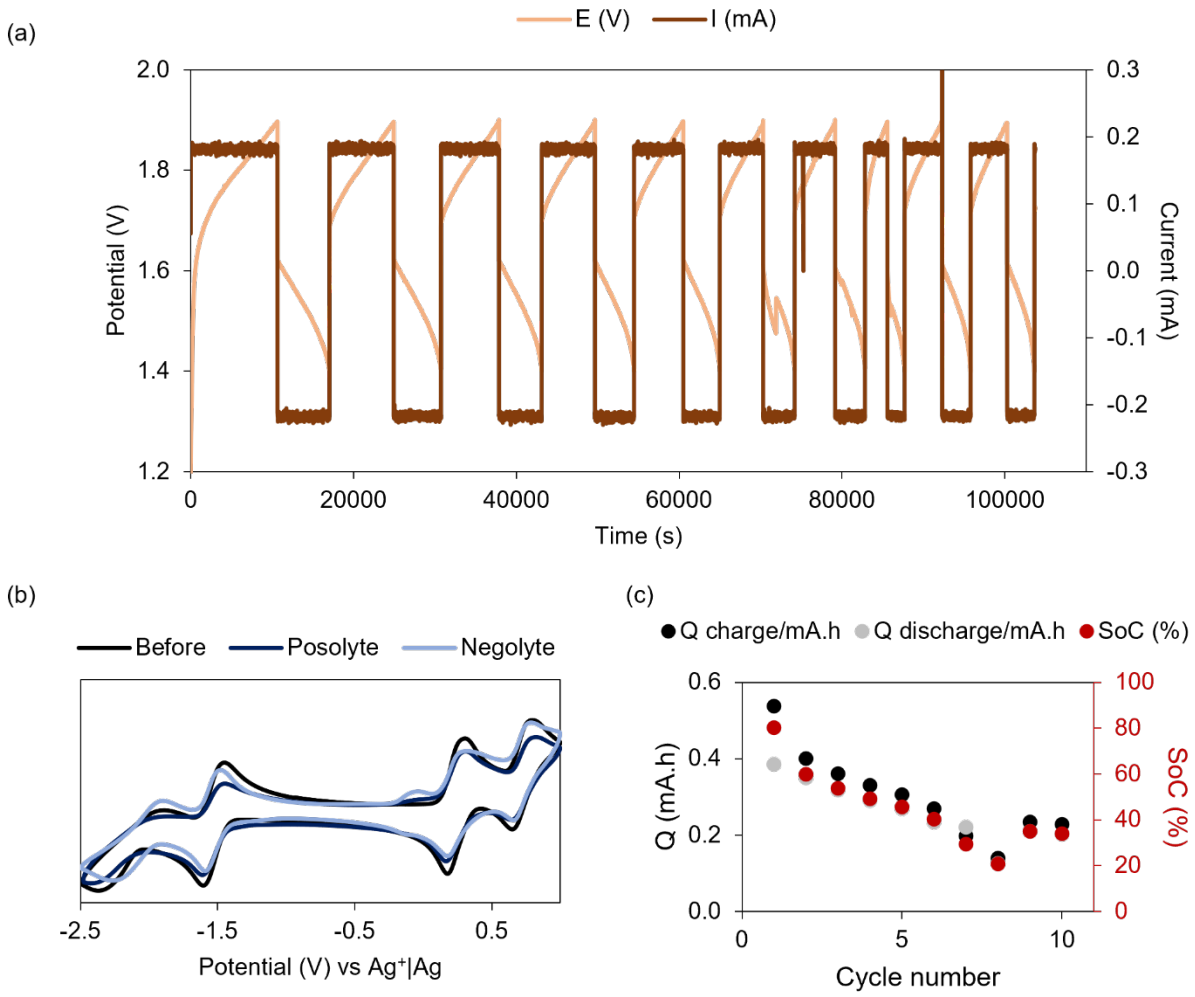

Figure S15. (a) Voltage trace of 10 cycles in charge–discharge cycling of **Ti_2V_4TRIOL^B** with *twice the volume* of negative electrolyte (b) Cyclic voltammograms of solutions after charge–discharge cycling (c) Capacity fade over 10 cycles (black circles represent charging capacity; grey circles represent discharging capacity). The spurious responses in (a) and outliers in cycles 7 and 8 in (c) correspond to interrupted stirring during battery cycling.

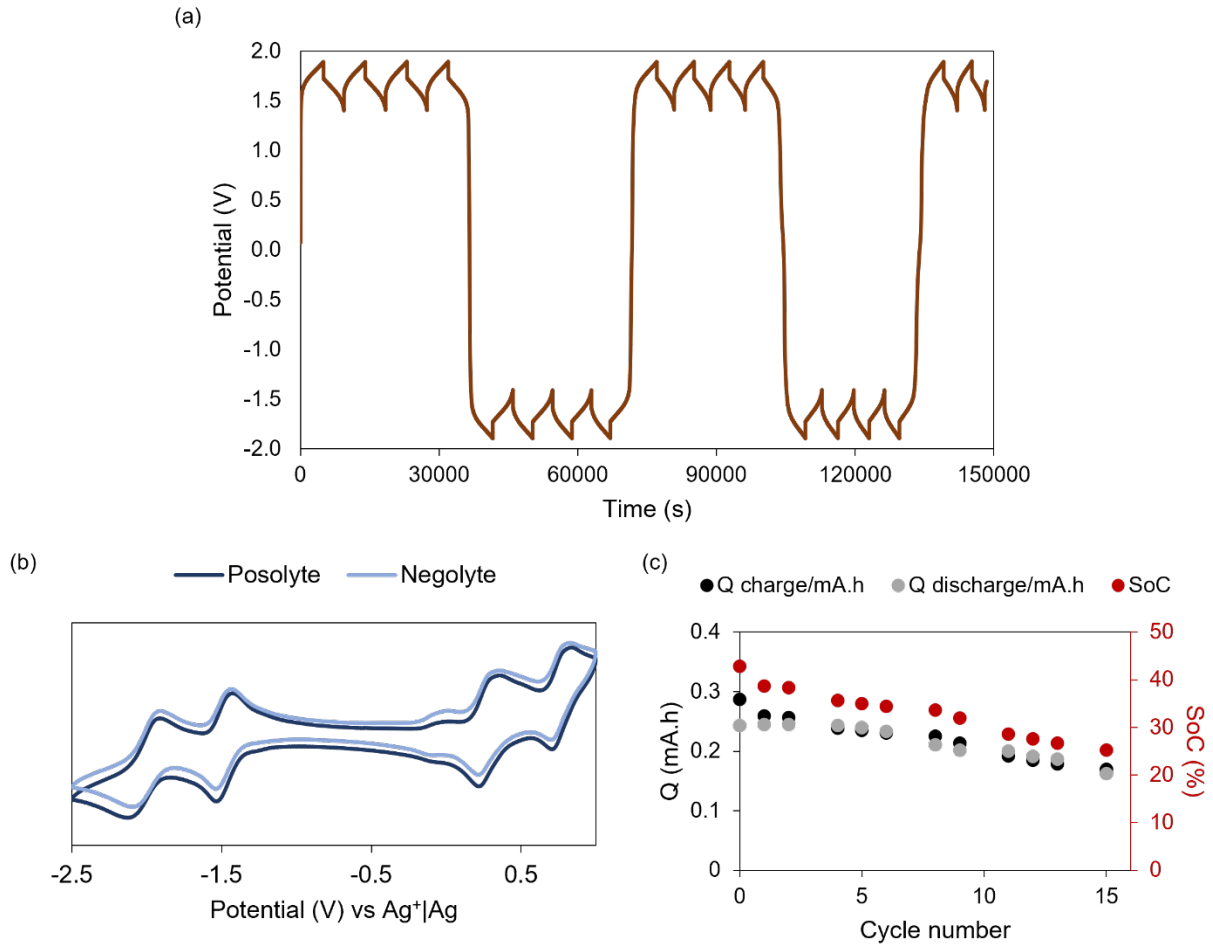

Figure S16. (a) Voltage trace of 15 charge-discharge cycles of $\mathbf{Ti_2V_4TRIOL^B}$ adopting the polarity swing technique (b) Cyclic voltammograms of solutions after charge–discharge cycling (c) Capacity fade observed for the 15 cycles. Note – The data points associated with cycles involving polarity switch are omitted for clarity. The black circles represent charging capacity; grey circles represent discharging capacity; red circles represent state-of-charge (SoC) of the battery.

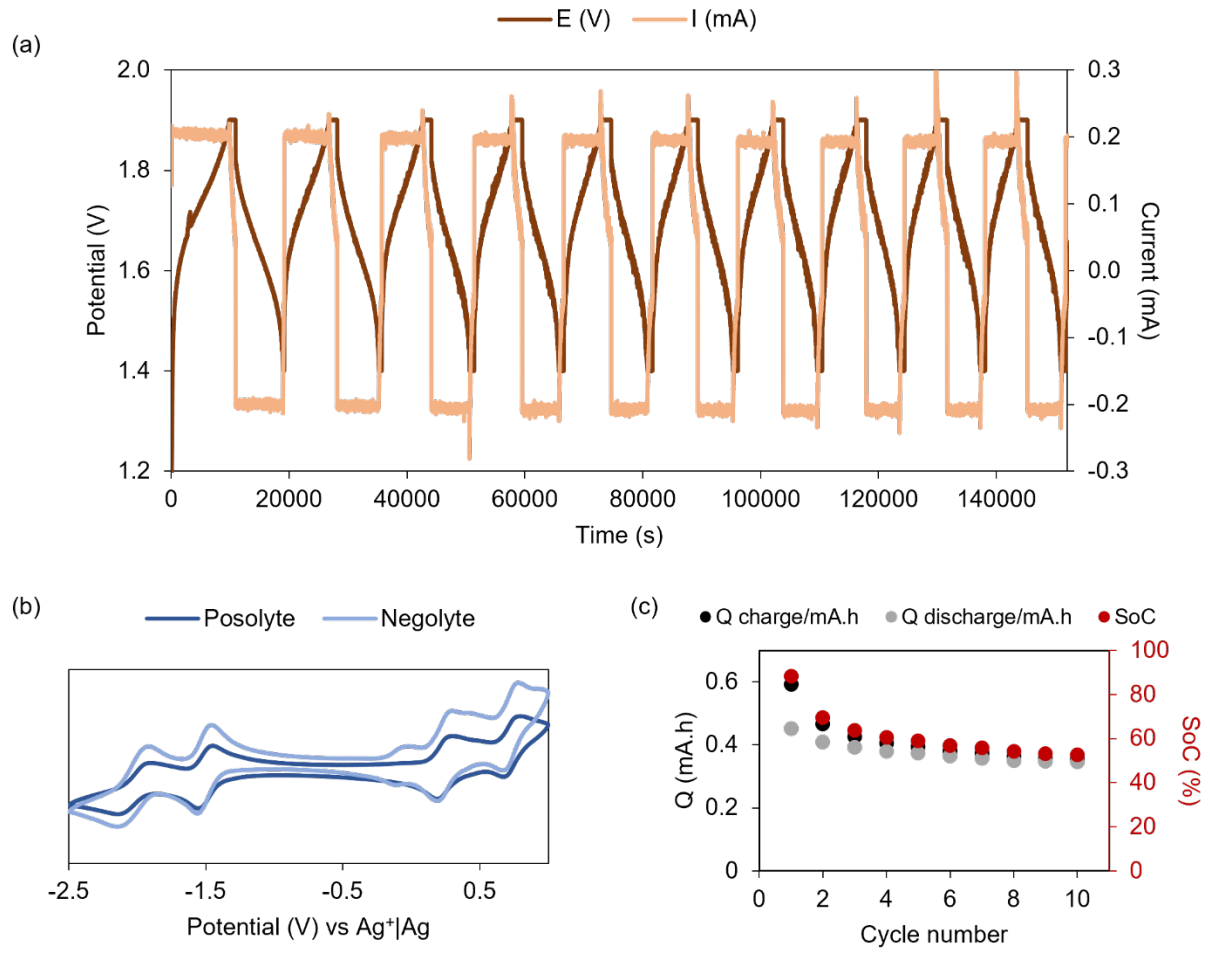

Figure S17. (a) Voltage trace of 10 cycles in charge–discharge cycling of **Ti_2V_4TRIOL^B** with *twice the concentration* of negative electrolyte (b) Cyclic voltammograms of solutions after charge–discharge cycling (c) Capacity fade over 10 cycles (black circles represent charging capacity; grey circles represent discharging capacity; red circles represent state-of-charge (SoC) of the battery). The spurious responses in (a) correspond to interrupted stirring during battery cycling.

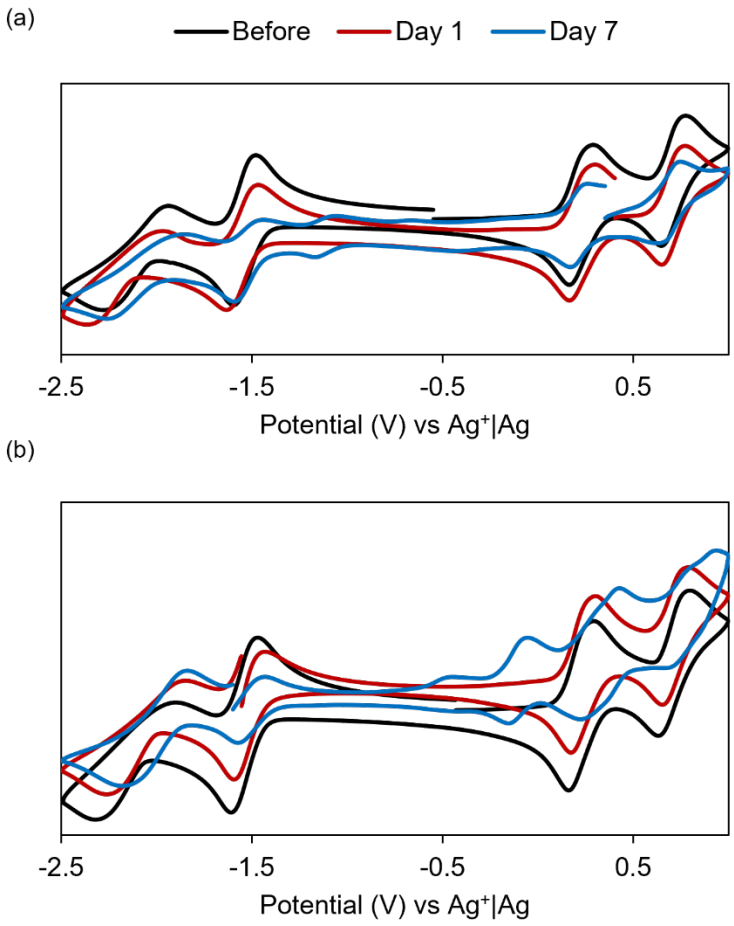

Figure S18. CV analysis post (a) bulk oxidation, and (b) bulk reduction for **Ti_2V_4TRIOL^B** and monitoring the solutions at 30^0C for 7 days. The breaks in the voltammograms indicate the open circuit voltage of the resulting solutions.

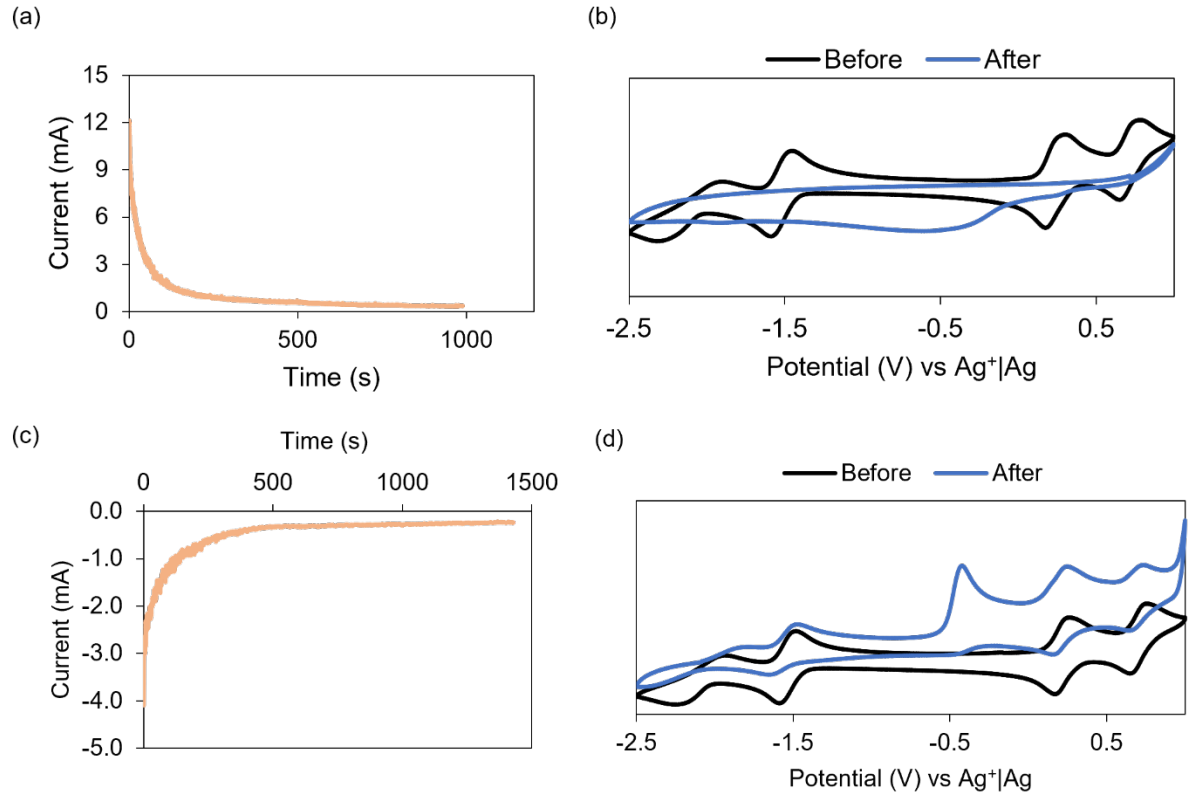

Figure S19. Instability of $\mathbf{Ti_2V_4TRIOL^B}$ to doubly charged states. Chronoamperometry (I-t) curves for bulk electrolysis to (a) +2 oxidation state (b) Cyclic voltammograms pre- and post-bulk oxidation; (c) and (d) represent corresponding bulk reduction measurements to -2 oxidation state.

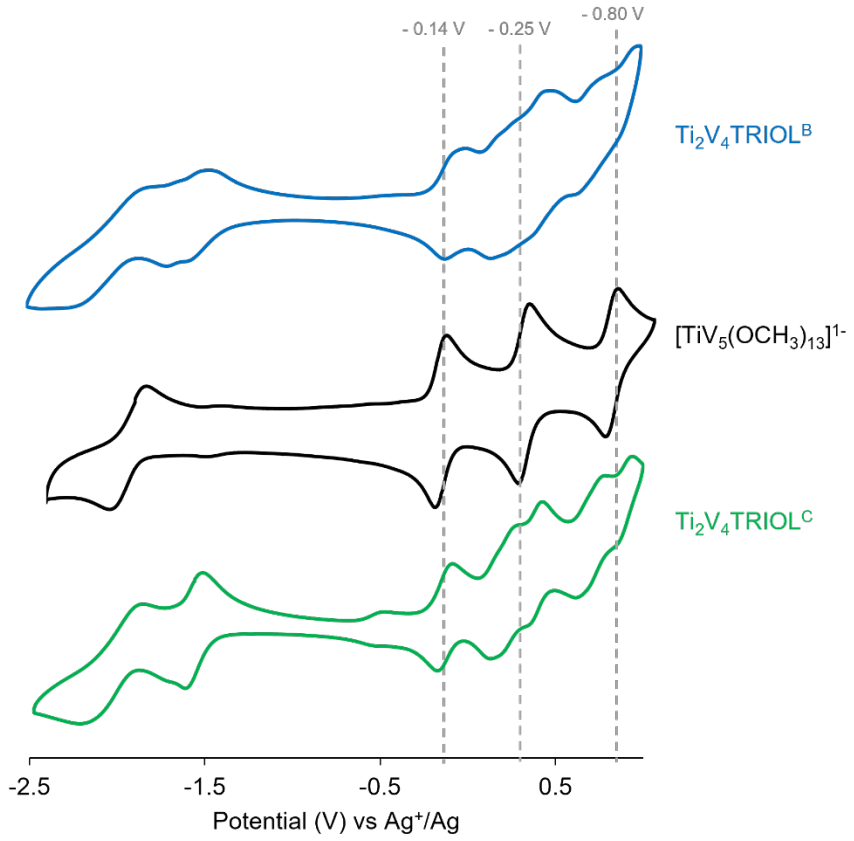

Figure S20. Cyclic voltammograms of the negative electrolyte for the compounds **Ti_2V_4TRIOL^B** and **Ti_2V_4TRIOL^C** after battery cycling compared to that of the proposed mono-titanium substituted POV-alkoxide impurity, $[TiV_5(OCH_3)_{13}]^{1-}$.

References

1. Q. H. Liu, A. E. S. Sleightholme, A. A. Shinkle, Y. D. Li and L. T. Thompson, *Electrochemistry Communications*, 2009, **11**, 2312-2315.
2. A. E. S. Sleightholme, A. A. Shinkle, Q. H. Liu, Y. D. Li, C. W. Monroe and L. T. Thompson, *Journal of Power Sources*, 2011, **196**, 5742-5745.
3. A. M. Kosswattaarachchi, L. E. VanGelder, O. Nachtigall, J. P. Hazelnis, W. W. Brennessel, E. M. Matson and T. R. Cook, *Journal of the Electrochemical Society*, 2019, **166**, A464-A472.
4. R. S. Nicholson, *Analytical Chemistry*, 1965, **37**, 1351-1355.